Journal of The Electrochemical Society, **155** (7) H504-H507 (2008)
0013-4651/2008/155(7)/H504/4/$23.00 © The Electrochemical Society

Triangular Extended Microtunnels in GaN Prepared by Selective Crystallographic Wet Chemical Etching

Hsin-Hsiung Huang,[a,b,z] Pei-Lun Wu,[a] Hung-Yu Zeng,[a] Po-Chun Liu,[b] Tung-Wei Chi,[b] Jenq-Dar Tsay,[b] and Wei-I Lee[a,z]

[a]*Department of Electrophysics, National Chiao Tung University, Hsinchu 30050, Taiwan*
[b]*Industrial Technology Research Institute, Hsinchu, 31040, Taiwan*

Extended microtunnels with triangular cross sections in thick GaN films were demonstrated using wet chemical etching on specially designed epitaxial lateral overgrowth structures. For tunnels along the $\langle 1\bar{1}00\rangle$ and $\langle 11\bar{2}0\rangle$ directions of GaN, the $\{11\bar{2}\bar{2}\}$ and $\{10\bar{1}\bar{1}\}$ facets are the etch stop planes with activation energies of 23 kcal/mol determined by wet chemical etching. The axial etching rate of the tunnels in the $\langle 1\bar{1}00\rangle$ direction is twice as large than that along the $\langle 11\bar{2}0\rangle$ direction. The highest etching rate of the tunnels in the axial direction is 1000 μm/h.
 [DOI: 10.1149/1.2913151]

Manuscript submitted January 14, 2008; revised manuscript received March 28, 2008. Available electronically May 8, 2008.

GaN and its alloys are widely employed on optoelectronic devices, such as light-emitting diodes (LEDs) and laser diodes (LDs), because they have a wide direct bandgap, high thermal stability, and unusual chemical stability. However, their excellent chemical stability also makes wet chemical etching difficult. Most methods of GaN etching involve dry etching processes such as reactive ion etching or inductively coupled plasma etching.[1-3] While dry etching has favorable characteristics, including a high etching rate and the ability to yield vertical sidewalls, it also has several disadvantages, including the damage caused by ion bombardment and the difficulty of obtaining smoothly etched sidewalls. Furthermore, tunnel structures buried in semiconductors cannot be realized by dry etching or photoenhanced electrochemical (PEC) techniques. Numerous research groups demonstrated PEC etching techniques,[4-16] but in most cases the etched surfaces of GaN were roughened.

In this article, extended microtunnels (EMTs) in GaN were prepared by wet chemical etching with an average etching rate of more than 15 μm/min. The etch stop facets of GaN EMTs are the $\{11\bar{2}\bar{2}\}$ or $\{10\bar{1}\bar{1}\}$ crystal planes, depending on the direction of the designed patterns of epitaxial lateral overgrowth (ELOG) directions. Several groups have tried to grow semipolar LEDs or LDs on $\{11\bar{2}2\}$, $\{10\bar{1}1\}$, and $\{10\bar{1}\bar{1}\}$ GaN crystal facets, which could result in higher-power or lower-threshold devices due to the reduced internal piezoelectric polarization field,[17-24] but the properties of these facets are still not clearly understood to this date. GaN EMTs are demonstrated in this report to further understand the etching properties of these facets. These microtunnels offer a channel for microfluid studies, especially in the applications of microelectromechanical systems.[25]

All of the samples herein consist of several tens of micrometers of GaN thickness grown by hydride vapor phase epitaxy (HVPE) on sapphire substrates. In the first growth process, a 4 μm thick GaN template was grown by metallorganic chemical vapor deposition on a (0001) *c*-plane sapphire substrate. The second growth process was the deposition of a 300 nm thick SiO_2 layer by plasma-enhanced chemical vapor deposition. Then, standard photolithography was performed to fabricate the stripes of a 5 μm wide SiO_2 mask separated by 5 μm wide windows in the $\langle 1\bar{1}00\rangle$ and $\langle 11\bar{2}0\rangle$ directions of GaN. Subsequently, the GaN layer with the patterned SiO_2 mask was used as an ELOG template for the regrowth of a thick GaN film of several tens of micrometers by HVPE at 1050°C. Ammonia gas was used as a nitrogen source and the GaCl generated by liquid Ga metal and HCl gas at 850°C was used as the Ga source. After the GaN regrowth by the HVPE system, the samples were sliced into small pieces for wet chemical etching, which was conducted in molten KOH between 170 and 250°C. Long-distance EMTs buried in GaN were obtained after wet chemical etching in the molten KOH.

Figure 1 shows scanning electron microscopy (SEM) images of the initial state of GaN EMT formation in the molten KOH. First, the SiO_2 layer was removed by the molten KOH. After the SiO_2 was removed, the GaN right above the SiO_2 mask region starts to be etched by the molten KOH. When the etchant reached the etch stop planes, the GaN EMTs formed. The etching mechanism of GaN EMTs by the molten KOH has been described in detail elsewhere.[26,27]

Figure 2 shows the cross-sectional SEM images of ELOG stripes in two directions after wet chemical etching. As presented in Fig. 2a and b, when the SiO_2 stripes were aligned in the $\langle 1\bar{1}00\rangle$ direction of GaN, the sidewall of GaN EMTs had a 58° angle after the wet chemical etching, corresponding to the $\{11\bar{2}\bar{2}\}$ crystal facets of GaN. As shown in Fig. 2c and d, when the SiO_2 stripes were aligned in the $\langle 11\bar{2}0\rangle$ direction, the sidewalls of the GaN EMTs were at 62°, corresponding to the $\{10\bar{1}\bar{1}\}$ crystal facets.

The depths of the GaN tunnels for two SiO_2 stripes in two directions were measured individually under an optical microscope. The etching rates of the tunnels differed in the axial direction, as shown in Fig. 3. The etching rate of the tunnels in the $\langle 1\bar{1}00\rangle$ direction substantially exceeds that in the tunnels in the $\langle 11\bar{2}0\rangle$ direction. The

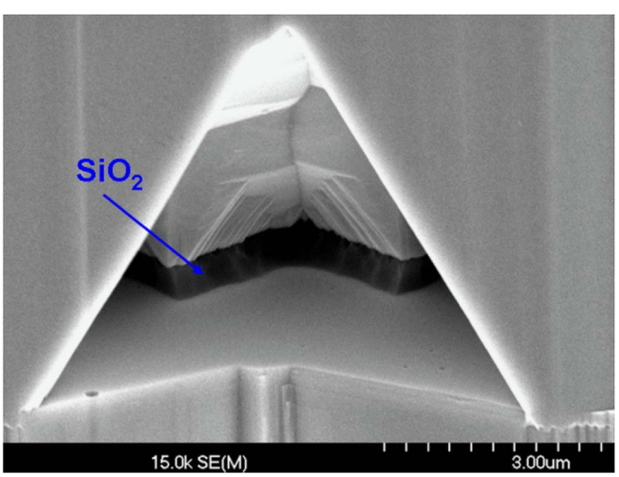

Figure 1. (Color online) Cross-sectional SEM image of the initial state of GaN tunnels along the $\langle 11\bar{2}0\rangle$ direction in the molten KOH etching.

[z] E-mail: hhhuang.9321803@nctu.edu.tw; wilee@cc.nctu.edu.tw

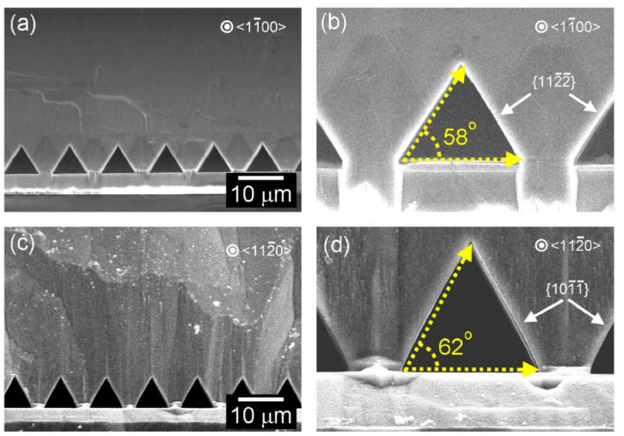

Figure 2. (Color online) SEM images of cross sections of GaN after the wet chemical etching. (a) Tunnels aligned along the ⟨1$\bar{1}$00⟩ direction. (b) Magnified image of one tunnel in the ⟨1$\bar{1}$00⟩ direction with an inclined angle of 58°. (c) Tunnels aligned in the ⟨11$\bar{2}$0⟩ direction. (d) Magnified image of one tunnel in the ⟨1$\bar{1}$00⟩ direction with an inclined angle of 62°.

average etching rate of the tunnels in the ⟨1$\bar{1}$00⟩ direction was as high as 15 μm/min at 250°C, and the average etching rate of the tunnels in the ⟨11$\bar{2}$0⟩ direction was only 15 μm/min at 250°C. The etching rate of the tunnels was highest in the ⟨1$\bar{1}$00⟩ direction, reaching 1000 μm/h in the initial 30 min of etching at 250°C.

Factors that may influence the etching rate of GaN EMTs include the width and thickness of the SiO_2 mask, the removal rate of the SiO_2 mask, the etching rate of the nitrogen-face GaN, and the etching rates of the various special crystal facets of GaN. The first three factors are the same for tunnels in different directions, so the factor that is most probably responsible for the variation in axial etching rates is the variation among etching rates of the {10$\bar{1}\bar{1}$} and {11$\bar{2}\bar{2}$} planes of GaN. The {10$\bar{1}\bar{1}$} family of planes of GaN is more stable and hardly etched by wet chemical etching than the {11$\bar{2}\bar{2}$} family of planes, mainly due to lower density of nitrogen atoms or surface energy.[28-33] The stability of the {10$\bar{1}\bar{1}$} family of planes makes the cross-section size of GaN EMTs along the ⟨11$\bar{2}$0⟩ direction larger

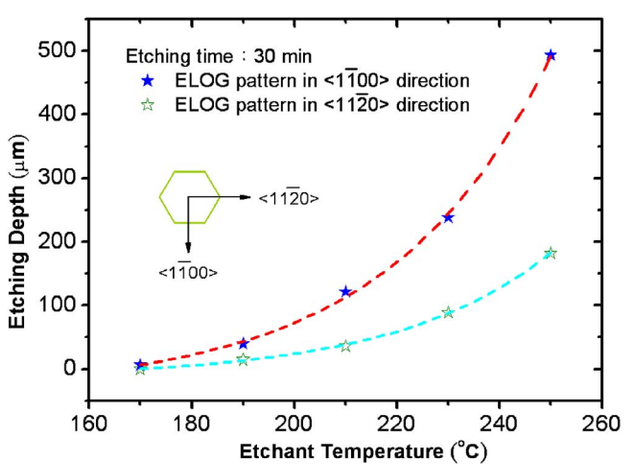

Figure 3. (Color online) Plot of the depth of GaN tunnels in different directions as a function of etchant temperature at a fixed etching time of 30 min in the molten KOH.

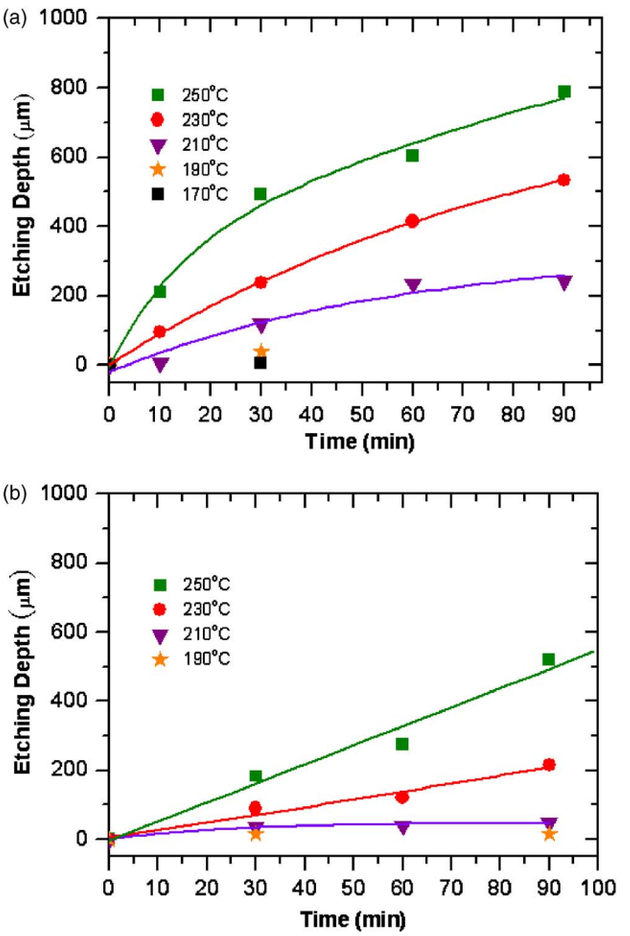

Figure 4. (Color online) Time dependence of the etching depth of GaN tunnels at various temperatures, with the ELOG pattern in the (a) ⟨1$\bar{1}$00⟩ and (b) ⟨11$\bar{2}$0⟩ direction.

than that along the ⟨1$\bar{1}$00⟩ direction. The etchant exchange in tunnels with larger cross section is easier than the small one. It makes the axial etching rate of tunnels along the ⟨11$\bar{2}$0⟩ direction lower than that in the ⟨1$\bar{1}$00⟩ direction.

Figure 4 plots the etching depths of GaN tunnels in two directions at various etching temperatures. The etching rate of GaN tunnels depended strongly on temperature. In this investigation, the etching temperature was between 170 and 250°C. When the etching temperature was below 190°C, the etching rate became very low in both directions of the tunnels. In Fig. 4a, the tunnels of GaN were aligned in the ⟨1$\bar{1}$00⟩ direction. The etching rate declined as the etching time increased, as presented in Fig. 4a. In the first 30 min of wet chemical etching at 250°C, the mean etching rate was higher than 15 μm/min. However, after 90 min of etching, the mean etching rate attenuated to 8 μm/min at the same temperature. Although the etching rate declined with the reaction time, it still exceeded that of dry or PEC etching. In Fig. 4b, the tunnels of GaN were aligned in the ⟨11$\bar{2}$0⟩ direction. The decline in the etching rate with the reaction time was not observed in these samples, and the etching rate of GaN tunnels was almost one-half of that of tunnels in the ⟨1$\bar{1}$00⟩ direction at the same temperature, because the etching rate of

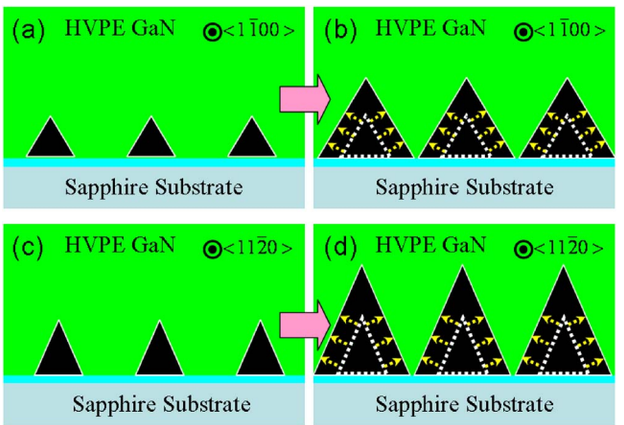

Figure 5. (Color online) Cross-sectional structure of GaN EMTs (a) beginning to form well-shaped triangular tunnels and (b) forming larger triangular tunnels upon facet etching.

the GaN tunnels along the $\langle 11\bar{2}0\rangle$ direction was much lower than that along the $\langle 1\bar{1}00\rangle$ direction, and no clear attenuation was observed during 90 min of reaction.

For understanding the characteristics of the $\{11\bar{2}2\}$ and $\{10\bar{1}\bar{1}\}$ planes of GaN, the etching rates and the activation energies in the molten KOH for the $\{11\bar{2}2\}$ and $\{10\bar{1}\bar{1}\}$ families of planes were determined in the GaN tunnels. First, all of the samples were etched by the molten KOH to form well-shaped triangular microtunnels, as presented in Fig. 5a and c. The chemical etching was then maintained to expand the tunnels, as shown in Fig. 5b and d. The etching rates of the $\{11\bar{2}2\}$ and $\{10\bar{1}\bar{1}\}$ families of planes were measured from the cross section of all samples. Figure 6 shows the Arrhenius plot of the $\{11\bar{2}2\}$ and $\{10\bar{1}\bar{1}\}$ families of planes of GaN. Two different etching rates were recorded at each temperature. The activation energies that corresponded to the $\{11\bar{2}2\}$ and $\{10\bar{1}\bar{1}\}$ facets were 23 kcal/mol. The activation energy of the $\{10\bar{1}\bar{1}\}$ and $\{11\bar{2}2\}$ facets of GaN indicated that the etching was reaction-rate-limited. If the etching rate had been diffusion-limited, the activation energy in the 1–6 kcal/mol range would be expected. The characteristics being

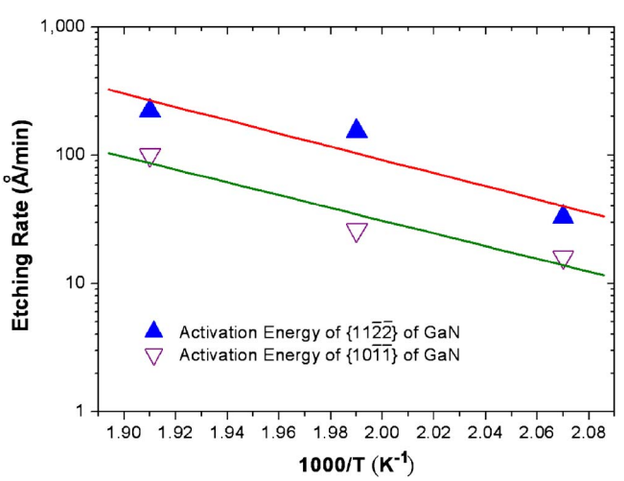

Figure 6. (Color online) Arrhenius plot of etching rates of two crystal facets of GaN. Solid and hollow dot symbols represent the etching rates on the $\{11\bar{2}2\}$ and $\{10\bar{1}\bar{1}\}$ crystal facets, respectively.

reaction-rate-limited implied a higher crystal quality.[34-37] The activation energy obtained herein can be compared with that obtained by Stocker et al.[35,38] They determined the activation energy of $\{10\bar{1}0\}$ and $\{10\bar{1}\bar{2}\}$ crystal facets of GaN. Their results are very close to those obtained herein.

In conclusion, extended microtunnels in different directions with triangular cross sections were formed in thick GaN films on specially designed ELOG structures. For tunnels in the $\langle 1\bar{1}00\rangle$ direction, the $\{11\bar{2}2\}$ family of planes were the etch stop planes, while for tunnels in the $\langle 11\bar{2}0\rangle$ direction, the $\{10\bar{1}\bar{1}\}$ family of planes were the more stable planes. The activation energies of wet chemical etching for the $\{11\bar{2}2\}$ family of planes and the $\{10\bar{1}\bar{1}\}$ planes were determined to be 23 kcal/mol. The $\{10\bar{1}\bar{1}\}$ family of planes were more stable and harder to etch than the $\{11\bar{2}\bar{2}\}$ family of planes. Consequently, the depths of the tunnels in the $\langle 1\bar{1}00\rangle$ direction were more than twice deeper than those along the $\langle 11\bar{2}0\rangle$ direction. The highest etching rate of the tunnels along the axial direction was 1000 μm/h. These straight triangular microtunnels with well-formed sidewalls may serve as a vehicle for microfluid applications.

Acknowledgments

The authors thank the National Science Council of the Republic of China, Taiwan, for financially supporting this work under contract no. 95–2622-E-009–011 and no. 96–2112-M-009–034, and the Ministry of Education of the Republic of China, Taiwan, for their financial support.

National Chiao Tung University assisted in meeting the publication costs of this article.

References

1. R. J. Shul, A. J. Howard, S. J. Pearton, C. R. Abernathy, and C. B. Vartuli, *J. Electrochem. Soc.*, **143**, 3285 (1996).
2. J. M. Lee, K. M. Chang, I. H. Lee, and S. J. Park, *J. Electrochem. Soc.*, **147**, 1859 (2000).
3. J. M. Lee, S. W. Kim, and S. J. Park, *J. Electrochem. Soc.*, **148**, G254 (2001).
4. C. Youtsey, L. T. Romano, R. J. Molnar, and I. Adesida, *Appl. Phys. Lett.*, **74**, 3537 (1999).
5. C. Youtsey, L. T. Romano, and I. Adesida, *Appl. Phys. Lett.*, **73**, 797 (1998).
6. C. Youtsey and I. Adesida, *Appl. Phys. Lett.*, **71**, 2151 (1997).
7. H. Peng and C. W. Chuang, *Appl. Phys. Lett.*, **72**, 939 (1998).
8. P. Visconti, K. M. Jones, and M. A. Reshchikov, *Appl. Phys. Lett.*, **77**, 3532 (2000).
9. M. Tiginyanu, V. Popa, and O. Volciuc, *Appl. Phys. Lett.*, **86**, 174102 (2005).
10. H. Lu, Z. Wu, and I. Bhat, *J. Electrochem. Soc.*, **144**, L8 (1997).
11. D. A. Stocker and E. F. Schubert, *J. Electrochem. Soc.*, **146**, 2702 (1999).
12. I. M. Huygens, K. Strubbe, and W. P. Gomes, *J. Electrochem. Soc.*, **147**, 1797 (2000).
13. H. Hartono, C. B. Soh, S. J. Chua, and E. A. Fitzgerald, *J. Electrochem. Soc.*, **154**, H1004 (2007).
14. Z. H. Hwang, J. M. Hwang, H. L. Hwang, and W. H. Hung, *Appl. Phys. Lett.*, **84**, 3759 (2004).
15. R. T. Green, W. S. Tan, P. A. Houston, T. Wang, and P. J. Parbrook, *J. Electron. Mater.*, **36**, 397 (2007).
16. J. A. Bardwell, J. B. Webb, H. Tang, J. Fraser, and S. Moisa, *J. Appl. Phys.*, **89**, 4142 (2001).
17. M. Funato, M. Ueda, Y. Kawakami, Y. Narukawa, T. Kosugi, M. Takahashi, and T. Mukai, *Jpn. J. Appl. Phys.*, **45**, L659 (2006).
18. T. J. Baker, B. A. Haskell, F. Wu, J. S. Speck, and S. Nakamura, *Jpn. J. Appl. Phys.*, **45**, L154 (2006).
19. H. Zhong, A. Tyagi, N. N. Fellows, F. Wu, R. B. Chung, M. Saito, K. Fujito, J. S. Speck, S. P. DenBaars, and S. Nakamura, *Appl. Phys. Lett.*, **90**, 233504 (2007).
20. T. J. Baker, B. A. Haskell, F. Wu, P. T. Fini, J. S. Speck, and S. Nakamura, *Jpn. J. Appl. Phys.*, **44**, L920 (2005).
21. K. Nishizuka, M. Funato, Y. Kawakami, Sg. Fujita, Y. Narukawa, and T. Mukai, *Appl. Phys. Lett.*, **85**, 3122 (2004).
22. H. Masui, T. J. Baker, R. Sharma, P. M. Pattison, M. Iza, H. Zhong, S. Nakamura, and S. P. DenBaars, *Jpn. J. Appl. Phys.*, **45**, L904 (2006).
23. A. Chakraborty, T. J. Baker, B. A. Haskell, F. Wu, J. S. Speck, S. P. Denbaars, S. Nakamura, and U. K. Mishra, *Jpn. J. Appl. Phys.*, **44**, L945 (2005).
24. A. Tyagi, H. Zhong, R. B. Chung, D. F. Feezell, M. Saito, K. Fujito, J. S. Speck, S. P. DenBaars, and S. Nakamura, *Jpn. J. Appl. Phys.*, **46**, L444 (2007).
25. V. Cimalla, J. Pezoldt, and O. Ambacher, *J. Phys. D*, **40**, 6386 (2007).
26. H. H. Huang, H. Y. Zeng, C. L. Lee, S. C. Lee, and W. I. Lee, *Appl. Phys. Lett.*, **89**, 202115 (2006).

27. H. H. Huang, H. Y. Zeng, and W. I. Lee, *Phys. Status Solidi B*, **244**, 1872 (2007).
28. J. E. Northrup and J. Neugebauer, *Phys. Rev. B*, **60**, R8473 (1999).
29. Y. Gao, M. D. Craven, and J. S. Speck, *Appl. Phys. Lett.*, **84**, 3322 (2004).
30. D. Zhuang and J. H. Edgar, *Mater. Sci. Eng., R.*, **48**, 1 (2005).
31. D. Li, M. Sumiya, S. Fuke, D. Yang, and D. Que, *J. Appl. Phys.*, **90**, 4219 (2001).
32. H. M. Ng, N. G. Weimann, and A. Chowdhury, *J. Appl. Phys.*, **94**, 650 (2003).
33. J. R. Mileham, S. J. Pearton, C. R. Abernathry, J. D. MacKenzie, R. J. Shul, and S. P. Kilcoyne, *Appl. Phys. Lett.*, **67**, 1119 (1995).
34. S. S. Tan, M. Ye, and A. G. Milnes, *Solid-State Electron.*, **38**, 17 (1995).
35. D. A. Stocker, I. D. Goepfert, E. F. Schubert, K. S. Boutros, and J. M. Redwing, *J. Electrochem. Soc.*, **147**, 763 (2000).
36. C. B. Vartuli, S. J. Pearton, J. W. Lee, C. R. Abernathy, J. D. MacKenzie, J. C. Zolper, R. J. Shul, and F. Ren, *J. Electrochem. Soc.*, **143**, 3681 (1996).
37. S. Adachi and K. Oe, *J. Electrochem. Soc.*, **131**, 126 (1984).
38. D. A. Stocker, E. F. Schubert, and J. M. Redwing, *Appl. Phys. Lett.*, **73**, 2654 (1998).